Journal of Photochemistry & Photobiology, B: Biology 221 (2021) 112250

Contents lists available at ScienceDirect

Journal of Photochemistry & Photobiology, B: Biology

journal homepage: www.elsevier.com/locate/jphotobiol

Photocatalytic degradation of drugs in water mediated by acetylated riboflavin and visible light: A mechanistic study

Alice Pavanello [a], Debora Fabbri [b], Paola Calza [b], Debora Battiston [b], Miguel A. Miranda [a], M. Luisa Marin [a,*]

[a] Instituto de Tecnología Química UPV-CSIC, Universitat Politècnica de València, E-46022 Valencia, Spain
[b] Dipartimento di Chimica, Università di Torino, via P. Giuria 5, 10125 Torino, Italy

ARTICLE INFO

Keywords:
Electron transfer
Organic dye
Photodegradation products
Singlet oxygen
Visible light

ABSTRACT

There is a current concern, among the scientific community, on the pollutants classified as "persistent organic pollutants (POPs)". Pharmaceuticals and personal care products (PPCPs) belong to this family of contaminants; therefore, it is necessary to find more efficient techniques able to achieve their removal from the environment. This study focuses on two different pharmaceuticals: carbamazepine and atenolol, chosen for their widespread use and their different chemical and medical properties. In this work, an organic dye, acetylated riboflavin, has been used in combination with visible light to achieve the photodegradation of these two POPs in <2 h. Moreover, photophysical experiments demonstrated the involvement of the singlet and triplet excited states of acetylated riboflavin and the generated singlet oxygen in the removal of these drugs. Besides, a detailed UFLC-MS-MS analysis of the photoproducts confirmed the oxidation of the drugs. Finally, a plausible mechanism has been postulated.

1. Introduction

In current life, pharmaceuticals and personal care products (PPCPs) are commonly found ingredients [1]. They comprise mainly organic molecules with different biological and toxicological properties that eventually end unaltered or partially metabolized spread in the sewage water. Recent works reported levels of PPCPs in untreated effluents range from ng/L to μg/L [2,3]. Although, they have been detected in concentrations far below the therapeutic doses, they could still have side effects on humans and/or wildlife, because they may chronically affect living organisms in different stages of development. Moreover, as they are in complex mixtures, they can participate in unknown processes giving rise to additional collateral effects [4,5].

Advanced oxidation processes (AOPs) are the basis of efficient approaches for the treatment of wastewater containing reluctant contaminants that are not degraded by conventional technologies. AOPs rely on the generation of reactive oxygen species (ROS), which can unselectively oxidize organic pollutants belonging to different chemical families. AOPs include different techniques, such as those based on ozone, radiolysis, UV, photo-Fenton, photocatalysis, *etc.* [6–8]. Among these methodologies, visible-light photoredox catalysis constitutes an environmentally green alternative, which has received considerable attention in the last years [9]. Among the advantages, the photocatalysts could absorb sunlight, which is a unique natural energy resource, abundant, non-polluting, cheap, clean and endlessly renewable [10]. Although metal-based photocatalysts such as $Ru(bpy)_3^{2+}$ have been widely explored, other kind of dyes, such as metal-free organic molecules are receiving increasing attention as greener options for the photocatalytic abatement of contaminants in wastewaters [11–15]. In this context, Riboflavin (RF) widely exists in fruits, vegetables or microorganisms, has been explored as a natural photocatalyst (Fig. 1) [16]. This dye absorbs visible light, generating excited states and reactive oxygen species (ROS), which can subsequently degrade pollutants *via* photocatalysis [17–19]. Although RF suffers degradation upon sunlight exposure, derivatization of the hydroxyl groups of the lateral chain as 2′,3′,4′,5′-tetraacetylriboflavin (RFTA) results in a marked improvement of its photochemical stability making it more appropriate for in-lab use (Fig. 1) [20–23].

To explore the potential of RFTA as an organic photocatalyst in the abatement of PPCPs, we have selected two currently used drugs that exhibit different chemical structures, and are administered for different medical diseases: carbamazepine (CBZ) and atenolol (ATN) (Fig. 1). Carbamazepine is a dibenzoazepine widely used as antiepileptic agent. Since

* Corresponding author.
E-mail address: marmarin@qim.upv.es (M.L. Marin).

https://doi.org/10.1016/j.jphotobiol.2021.112250
Received 13 February 2021; Received in revised form 2 June 2021; Accepted 26 June 2021
Available online 29 June 2021

it is readily biotransformed in the liver, it mostly arrives in the environment after conversion into its metabolites [24]. It is resistant not only to natural bio and photo-reactions but also to the conventional wastewater treatment plants, so it is easily detectable in the environmental aqueous systems: some studies proved that carbamazepine is one of the most resilient pharmaceuticals in the environment [25,26]. Atenolol is one of the most extensively used β-blocker drug: it is administered to treat cardiovascular diseases, coronary heart disease, hypertension, sinus tachycardia, arrhythmias or myocardial infarction [27]. Although recent reports have shown that atenolol is unlikely to cause acute toxicity at low concentrations, this drug is persistent in the environment due to its high stability and continuous release as a result of extensive human use [28].

With this background, in this contribution we have investigated the photocatalytic potential of RF derivatives to remove carbamazepine and atenolol from the environment, with special stress on the mechanistic details. To improve the stability of RF it has been used as RFTA and a solar simulator with a filter to remove UV and prevent direct photolysis of the drugs has been employed. Interestingly, photophysical experiments have allowed determining the role of the two excited states of RFTA and singlet oxygen in the postulated photodegradation mechanism.

2. Experimental

2.1. Chemicals

Carbamazepine, atenolol and 2,4,6-triphenylpyrylium tetrafluoroborate (TPP) were from TCI Chemicals and Sigma-Aldrich. Acetonitrile was from Scharlau. Acetylated riboflavin was synthetized from commercial Riboflavin (from TCI Chemicals) [21]. Water was Milli-Q grade. All other reagents were of analytical grade and used as received.

2.2. Photodegradation Experiments and Analytical Procedures

Aqueous solutions (5 mL) containing 10 mg L^{-1} of every drug and 1 mg L^{-1} of RFTA (from a stock solution of 50 mg L^{-1} in acetonitrile) underwent irradiation in cylindrical closed Pyrex cells under stirring (40 mm i.d. 25 mm high) using a 1500 W Xenon lamp and a cutoff filter at 400 nm. The concentration of substrates over time was tracked using a Merck-Hitachi HPLC with a L-4200 UV–Vis detector and a reverse-phase RP-C18 column (Lichrospher, 4 mm i.d. × 12.5 mm length and 5 μm particle diameter from Merck). Elution was carried out in isocratic conditions using phosphoric acid (3 mM) and acetonitrile with a ratio 65:35 *v*/v for CBZ and RFTA, and 40:60 v/v for ATN at 1 mL min^{-1} flow rate. ATN, CBZ and RFTA were detected at 215 nm, 285 nm and 460 nm, respectively.

Separation and identification of the intermediate photoproducts were carried out by a UFLC-SHIMADZU combined with QTRAP LC-MS/MS 3200 from SCIEX (Framingham, MA, USA). Electrospray ionization (ESI) was used in positive ion mode (50–600 *m/z* range) and the operating parameters for each molecule were reported in the Supplementary information (Section 1 UFLC-MS procedures).

The phototransformation products were tentatively identified based on their MS^2 spectra collected by enhanced product ions (EPI) mode, which was triggered by enhanced mass resolution (EMS) and enhanced resolution (ER) steps in agreement with the information depend acquisition (IDA) mode with a threshold of 500,000 cps.

Additional experimental data were obtained irradiating aqueous solutions (10 mL) containing 10 mg L^{-1} of every drug and 1 mg L^{-1} of RFTA in H_2O and D_2O under LED lamps centred at 460 nm. Moreover, aqueous solutions (10 mL) containing 10 mg L^{-1} of every drug and 1 mg L^{-1} of TPP were irradiated under lamps centred at 420 nm. All the solutions were irradiated in test tubes under air. Aliquots of 0.5 mL of treated solution were sampled at different irradiation times and analyzed at the UPLC-HRMS to identify the main photoproducts. The concentration of substrates over time was tracked using an HPLC instrument (Agilent 1100 Series model with quaternary pumpG1311 A, photodiode detector VWD G1314 A, standard liquid auto-sampler G1313 A and degasser G1322 A). A Teknokroma C18 Mediterranea Sea analytical column (25 × 0.46 mm and 5 μm particle size) was used and a mixture of acetonitrile/water was used as eluent working in isocratic mode (70% acetonitrile:30% H_2O pH 3 at a flow rate of 1 mL

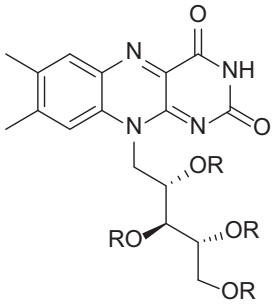

R	Name
-H	Riboflavin (RF)
$-COCH_3$	Acetylated Riboflavin (RFTA)

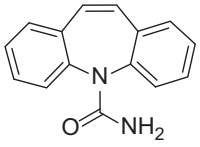

Carbamazepine

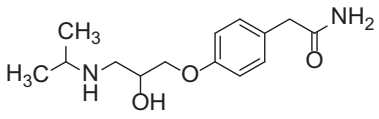

Atenolol

Fig. 1. Structure of Riboflavin (RF), Acetylated Riboflavin (RFTA), Carbamazepine (CBZ) and Atenolol (ATN).

min^{-1} for CBZ and 20% acetonitrile:80% H_2O pH 3 at a flow rate of 0.8 mL min^{-1} for ATN).

Exact mass values were determined by means of a QToF spectrometer coupled with a liquid chromatography system. Separations were accomplished by UPLC on a Zorbax Eclipse Plus C18 column (4.6 × 100 mm, 3.5 μm). See more details in the Suplementary Material Section 2.

2.3. Toxicity Tests

To evaluate the acute toxicity through the process, the samples taken at different irradiation times were submitted to a Microtox Model 500 Toxicity Analyzer (Milan, Italy). This bioluminescence inhibition assay monitors the natural emission changes of the marine bacterium *Vibrio fischeri* in the presence of toxic substances. Freeze-dried bacteria, reconstitution solution (2% NaCl) and an adjustment solution (non-toxic NaCl 22%) were obtained from Azur (Milan, Italy). Luminescence was recorded after 5, 15, and 30 min of incubation at 15 °C. Since no significant variations were observed among the three contact times, only the results corresponding to 5 min are given. The percentage of luminescence inhibition was calculated by comparison with a toxic-free control according to the accepted protocol by means of the Microtox calculation program.

2.4. Photophysical Experiments

For the steady-state and time-resolved fluorescence experiments, a Photon Technology International (PTI) LPS-220B and an EasyLife V (OBB) fluorimeter were used, respectively. Time-resolved fluorescence was measured upon excitation at 460 nm with a diode LED, using a cutoff filter (50% transmission at 475 nm). All the solutions were prepared in aerated acetonitrile with absorbance lower than 0.15 at 460 nm. Fluorescence quantum yield (Φ_F) for RFTA in acetonitrile was obtained using RF in water as a standard ($\Phi_F = 0.26$) [29,30]. Φ_{isc} was calculated as 1- Φ_F. A pulsed Nd:YAG SL404G-10 laser (Spectron Laser Systems) was used for the laser flash photolysis experiments ($\lambda_{excitation}$ = 355 nm, 20 mJ $pulse^{-1}$). The laser flash photolysis system was formed by the described laser, a pulsed Lo255 Oriel Xenon lamp, a 77,200 Oriel monochromator, an Oriel photomultiplier tube (PMT) housing, a 70,705 PMT power supply and a TDS-640A Tektronix oscilloscope. Experiments were performed using acetonitrile solution under nitrogen atmosphere with absorbance *ca.* 0.3 at 355 nm. Singlet oxygen quenching experiments were performed with the same LFP equipped with a Hamamatsu NIR emission detector. The characteristic emission signal of $^1O_2$ was monitored at 1270 nm upon increasing concentrations of drugs in aerated acetonitrile. Quartz cuvettes of 1 × 1 cm were used for all the photophysical experiments, which were performed at 298 K.

3. Results and Discussion

3.1. Photodegradation of RFTA

Preliminary irradiation tests were performed on RFTA aimed to establish its degradation rate and acute toxicity over time under visible light (with a filter at 420 nm) and are shown in Fig. 2. The complete disappearance of RFTA occurred within 2 h, whereas RFTA toxicity was very low (EC50 calculated for RF in water was 195 mg L^{-1}) and no significant changes in the acute toxicity were observed during the irradiation, so suggesting that under these experimental conditions, the toxicity effects both RFTA and its phototransformation products are low. Photodegradation of RFTA could not be considered a drawback for photocatalytic wastewater remediation, since natural incomes of vitamin B could be compensating the loss of the photocatalyst.

Along with RFTA degradation, six main phototransformation products were formed and detected by LC-MS; MS^2 product ions and proposed chemical structures are reported in Table S1. The compound **558** with *m/z* 559 is consistent with an oxidation of the molecule that can

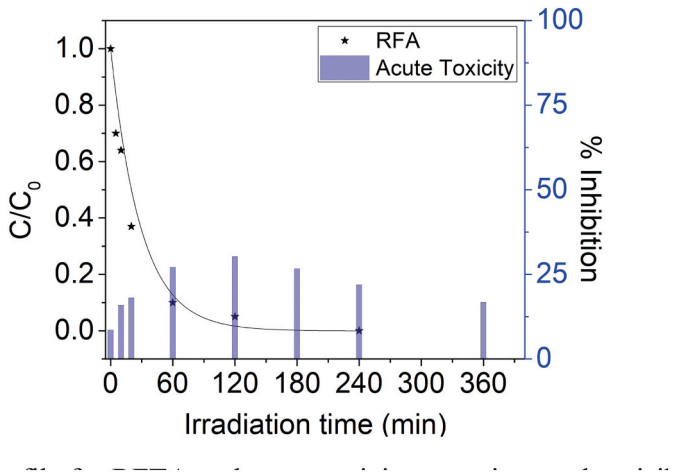

Fig. 2. Degradation profile for RFTA and acute toxicity over time under visible light irradiation.

involve one of the methyl groups on aromatic moiety, taking into account the similarity (correspondence) of fragmentation pattern occurring on the allylic structures with the RFTA molecule. Analogous considerations can be remarked for compound **574** arising from a further hydroxylation that could take place on the isoalloxazine structure. Hydroxy-byproducts were not detected in previous works investigating the phototransformation of RF [31] and its derivatives [32]. An alternative route of degradation involves the loss of *N*-alkyl substituent, which is supported by the detection of 7,8-dimethylalloxazine (photoproduct **242**), generally identified also as the main transformation product for RF photodecomposition (Lumichrome) [33,34]. The data obtained for phototransformation products **461**, **413** and **415** seem to involve the rupture of the ring and the side chain. The cleavage of the pyrimidine ring to form quinoxaline derivatives has been previously reported for photodegradation of RF products [35].

3.2. Phototransformation of Pharmaceuticals in the Presence of RFTA

Next, solutions of RFTA containing one of the pharmaceuticals were irradiated in a solar simulator with a 420 nm filter to ensure that only RFTA absorbs (see UV–visible spectra of each drug and RFTA, Fig. 3A–C), and the abatement of the drugs and RFTA was monitored *vs* time (Fig. 3D).

As shown in Fig. 3D, photocatalyzed degradation of the investigated drugs by RFTA proceeded efficiently under visible light in short times.

For instance, removal of up to 85% of CBZ in the presence of RFTA was accomplished within 10 min, while it is scarcely abated in wastewater treatment plants [26,36,37]. The removal of ATN was slower, but its initial concentration decreased to a 30% after 20 min of irradiation. Moreover, the complete abatement of CBZ and ATN occurred in 20 min and 120 min, respectively. The stability of RFTA was enhanced in the presence of the drugs, although eventually it was completely photodegraded after 120 min of irradiation.

Furthermore, all the irradiated samples were analyzed by LC-MS in order to identify the main transformation products. For CBZ, five photodegradation products were detected whose *m/z* and corresponding proposed structures are shown in the Table S2. The structural assignment was performed on the basis of MS^2 spectra and the data reported in the literature about the transformation products obtained upon treatment by different AOPs [24,38]. The possible transformation mechanism of CBZ is outlined in Scheme 1 and accounts basically for hydroxylation of the drug with the formation of two isobaric species, namely **252A** and **252B**. For the **252B**, the formation of hydroxycarbamazepine can be hypothesized, whereas the compound **252A**, *N*-aminocarbonylacridine-9-carboxaldehyde, would probably derive from

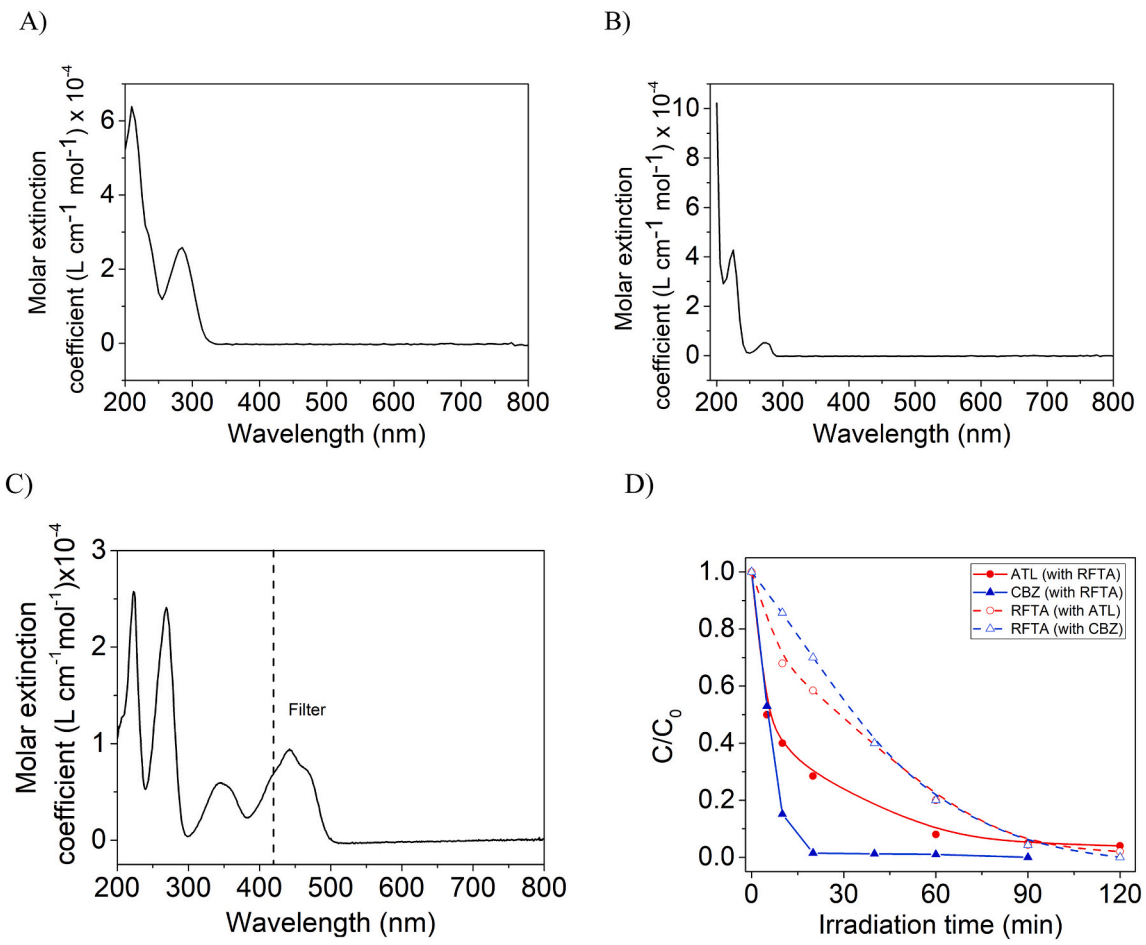

Fig. 3. UV–Vis spectra of (A) Carbamazepine, (B) Atenolol, and (C) Acetylated Riboflavin in aqueous solutions. (D) Disappearance of drugs in the presence of RFTA (solid traces and symbols) and evolution of the concentration of RFTA in each experiment (dashed traces and empty symbols): Carbamazepine (blue), Atenolol (red). (For interpretation of the references to colour in this figure legend, the reader is referred to the web version of this article.)

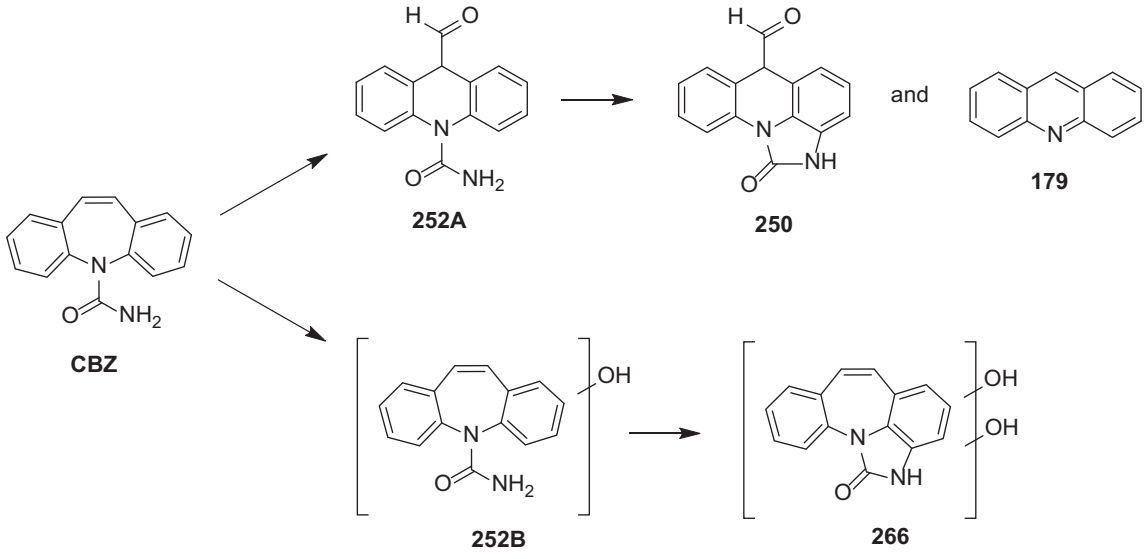

Scheme 1. Proposed pathway for the phototransformation of CBZ assisted by RFTA.

hydroxylation and ring contraction of CBZ, as previously observed [24,39]. An intramolecular cyclization occurring on **252A** would lead the formation of **250** and acridine (**179**) [24]. The proposed structure for photoproduct **266** is consistent with a double hydroxylation of CBZ with concomitant cyclization. However, structures of quinonoid derivatives of CBZ for **250** and **266** as suggested by Martinez et al. cannot be excluded [38].

During the phototransformation of ATN in the presence of RFTA,

four products were detected and identified (see Table S3) thanks to MS^2 obtained data and the support of literature [40–42]. The photoinduced transformation of this drug (Scheme 2) occurs by: (1) hydroxylation, leading to the formation of **282** [40]; (2) loss of amide group and the formation of a keto derivative (**237**), also detected by Radijenovic et al. [41] upon solar photocatalytic ATN degradation and justified by addition of oxygen to the benzylic radical; and (3) detachment of alkyl chain, *O*-dealkylation, leading to 3-(isopropylamino)propane-1,2-diol (**133**) [40,42]. A further oxidation of **282** would give **280** [41].

3.3. Singlet Excited State Involvement

The possible involvement of the singlet-excited state of RFTA in the photodegradation of the drugs was evaluated on the basis of fluorescence measurements. Actually, both the emission intensity and the lifetime of RFTA decreased with the increasing drug concentration (Fig. 4). The Stern-Volmer constants (K_{SV}) were determined from steady-state experiments according to Eq. (1). Furthermore, the quenching rate constants (k_{qs}) were determined from time-resolved experiments, applying another expression of the Stern-Volmer relationship (Eq. (2)) (Table 1). High values for the quenching constants k_{qS} were obtained for both drugs. If the quenching was only dynamic $K_{SV} = k_{qs}\,\tau_S$; nevertheless, in the case of CBZ and ATN the values determined for K_{SV} are much higher than the corresponding $k_{qs}\,\tau_S$, indicating partial contribution of the static mechanism in the quenching of the singlet excited state of RFTA (*i.e.* formation of a ground-state complex) [43].

$$I_0/I = 1 + K_{SV}\,[Q] \quad (1)$$

$$\tau_0/\tau = 1 + k_{qs}\,\tau_S\,[Q] \quad (2)$$

3.4. Triplet Excited State Participation

Laser flash photolysis (LFP) measurements allowed investigating the contribution of the excited triplet state to the photodegradation processes.

Initially, the typical signal corresponding to the triplet-triplet transition of RFTA (a band peaking at 380 nm and a broad absorption in the region 500–700 nm) was observed upon LFP of RFTA in deaerated acetonitrile (Fig. 5).

Next, LFP experiments were carried out in the presence of the drugs. Firstly, the transient absorption spectrum of RFTA and carbamazepine (2×10^{-2} M) is shown in Fig. 6A. Some triplet excited state was still present, as revealed by the shape of the region between 500 nm and 700 nm. Increasing concentrations of carbamazepine accelerated the decay at 680 nm; however, the quenching of ^{3}RFTA* seems slow, in fact the rate constant k_{qT} determined at 680 nm was 9.1×10^6 M^{-1} s^{-1} (Fig. 6B and C).

At 380 nm, increasing concentrations of carbamazepine at the beginning led to a faster decay, but after some μs the decay was slowed down; this tendency revealed the presence at 380 nm of two species. As a matter of fact, the fast decay could be related to the quenching of the triplet, while the longer-lived signal could be related to the formation of RFTAH$^\bullet$, the protonated radical anion of RFTA, suggesting an electron transfer oxidation of the drug under these conditions. Unfortunately, the signals of triplet and RFTAH$^\bullet$ could not be resolved in the transient absorption spectrum, since they overlap at 380 nm.

In the case of atenolol (Fig. 7), the situation was similar: the transient absorption spectrum of RFTA and atenolol (1.9×10^{-3} M) presented again two signals, one of them in the region 500–700 nm and the other centered at 380 nm (Fig. 7A).

In particular, the quenching of ^{3}RFTA* was studied at 680 nm (Fig. 7B). A progressive shortening of the decay was observed with the increasing drug concentration. From the Stern-Volmer plot (Fig. 7C), a k_{qT} value of 3.7×10^8 M^{-1} s^{-1} was determined. At 380 nm, as in the case of CBZ, the growth of a new signal was observed upon addition of ATN, which could be assigned to RFTAH$^\bullet$, the reduced species of the photocatalyst. Hence, quenching of the triplet excited state of RFTA happens by an electron transfer mechanism.

3.5. Singlet Oxygen Involvement

Laser flash photolysis (LFP) was also useful for the investigation of the role of O_2 in the photodegradation of CBZ and ATN. First, from the quenching of ^{3}RFTA* by O_2, a quenching constant value of $k_{qTO2} = 9.5 \times 10^9$ M^{-1} s^{-1} was determined (Fig. S1).

Next, the interaction of the drugs and $^1O_2$ was investigated. $^1O_2$ was obtained from a solution of RFTA in aerated acetonitrile upon laser flash photolysis excitation ($\lambda_{exc} = 355$ nm) and its typical phosphorescence was recorded at 1270 nm *vs* time in the presence of CBZ and ATN, at different concentrations. The quenching rate constants were determined for both drugs ($k_{q1O2} = 6.4 \times 10^5$ M^{-1} s^{-1} for CBZ and $k_{q1O2} = 1.4 \times 10^7$ M^{-1} s^{-1} for ATN) from the respective Stern-Volmer plots (Fig. 8).

3.6. Overall Discussion

The quenching of the ^{1}RFTA*, ^{3}RFTA* and $^1O_2$ by CBZ an ATN has been demonstrated through photophysical experiments. Even more, formation of RFTAH$^\bullet$ resulting from e^- transfer followed by H^+ transfer has been evidenced in the absence of O_2. The relative weight of the different reaction pathways in the photodegradation of the drugs has been evaluated based on the determined quenching constants *versus* drugs concentration, using acetonitrile as solvent to provide higher dynamic range.

First, we calculated the contribution of the singlet excited state of RFTA at different drugs concentration, according to the following equa-

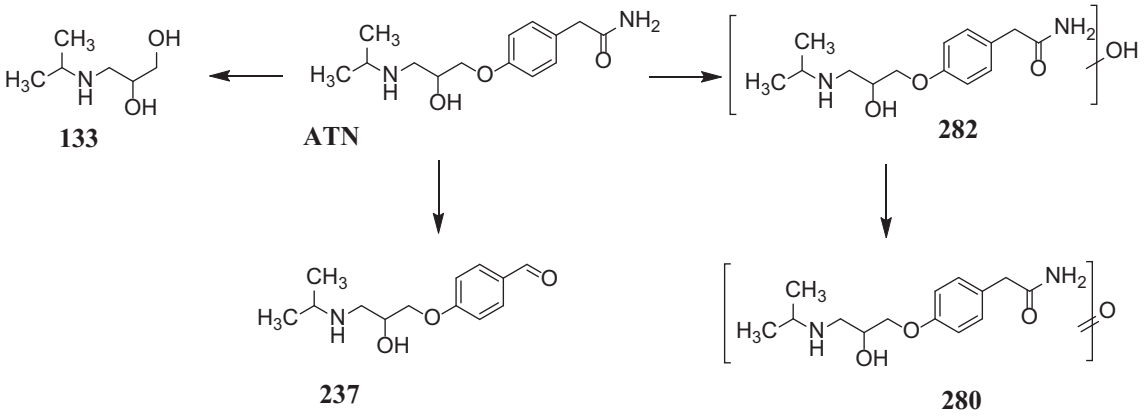

Scheme 2. Proposed phototransformation route of ATN in the presence of RFTA.

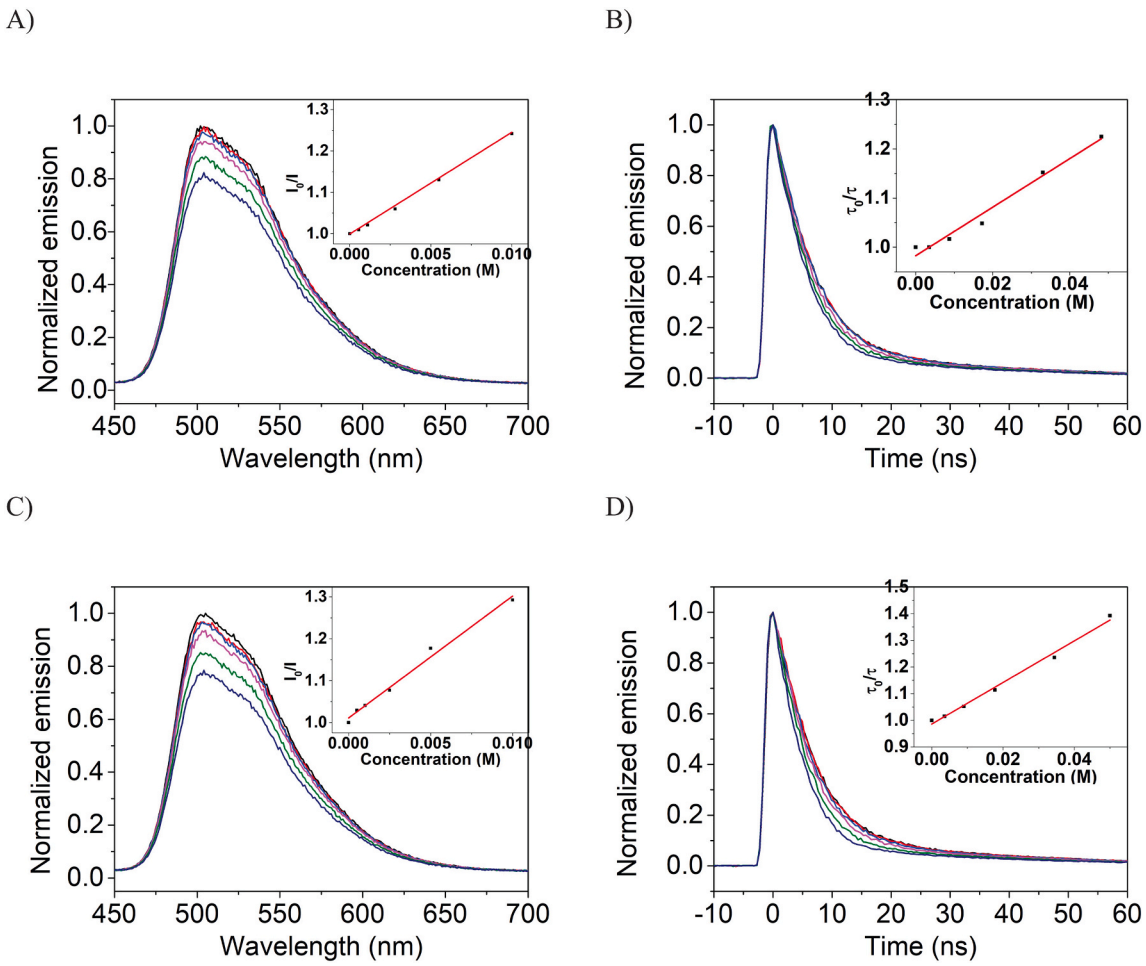

Fig. 4. Steady-state (left) and time-resolved emission (right) quenching experiments of RFTA upon increasing concentrations of CBZ (A and B) and ATN (C and D), in aerated CH_3CN. λ_{exc} = 445 nm for steady-state and λ_{exc} = 460 nm for time-resolved experiments.

Table 1
Constants for the quenching of ^{1}RFTA* by the drugs determined from steady-state (Stern-Volmer constant) and time-resolved measurements (rate constant).

Drugs	K_{SV} (M^{-1})	k_{qs} (M^{-1} s^{-1}) from time-resolved measurements
Carbamazepine (CBZ)	24.62	6.7×10^8
Atenolol (ATN)	29.15	1.1×10^9

tions:

$$Quenching\ of\ {}^{1}(RFTA)^{*}(\%) = \frac{k_{qs}[Q]}{\frac{\Phi_F}{\tau_s} + \frac{\Phi_{isc}}{\tau_s} + k_{qs}[Q]} x\ 100 \quad (3)$$

$${}^{1}(RFTA)^{*}\ intrinsic\ decay\ (\%) = \frac{\frac{\Phi_F}{\tau_s}}{\frac{\Phi_F}{\tau_s} + \frac{\Phi_{isc}}{\tau_s} + k_{qs}[Q]} x\ 100 \quad (4)$$

where: k_{qs} is the quenching constant of the singlet excited state of RFTA, [Q] is the concentration of the pollutants, Φ_F and Φ_{isc} are the quantum yields of fluorescence and intersystem crossing and τ_s is the lifetime of the singlet excited state of RFTA.

Next, the quenching of the ^{3}RFTA* and the intrinsic decay of ^{3}RFTA* were calculated according to the following equations:

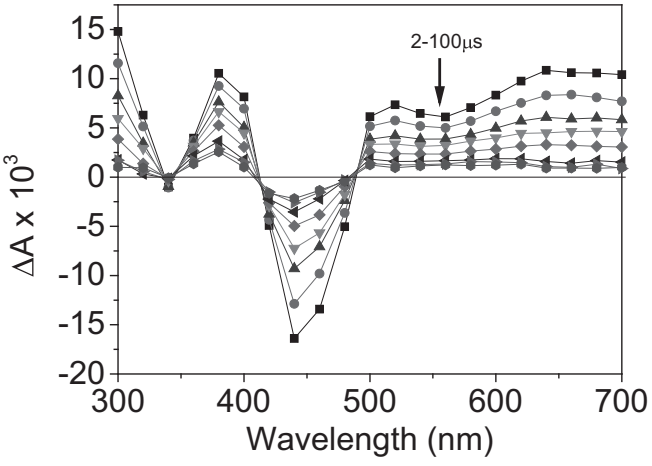

Fig. 5. Transient absorption spectra of RFTA recorded at different delay times after the 355 nm laser shot in deaerated acetonitrile (absorbance *ca.* 0.3 at the excitation wavelength).

$$Quenching\ of\ {}^{3}(RFTA)^{*}(\%) = \frac{\frac{\Phi_{isc}}{\tau_s}}{\frac{\Phi_F}{\tau_s} + \frac{\Phi_{isc}}{\tau_s} + k_{qs}[Q]} x \frac{k_{qT}[Q]}{\frac{1}{\tau_T} + k_{qT}[Q] + k_{O_2T}[O_2]} x100 \quad (5)$$

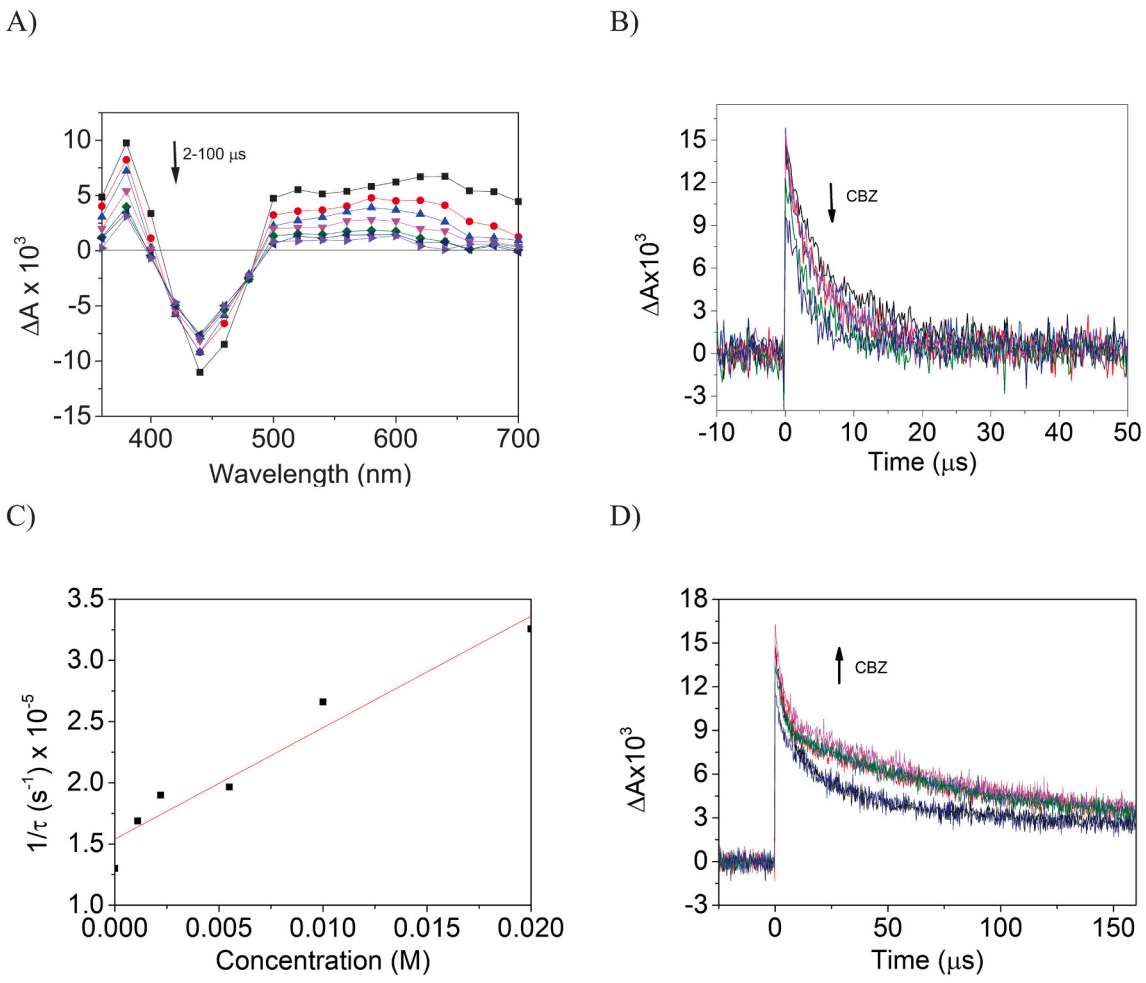

Fig. 6. LFP of RFTA in the presence of carbamazepine (2×10^{-2} M), recorded at different times after the laser pulse from 350 nm to 700 nm, ($\lambda_{exc} = 355$ nm) (A). Transient absorption decays of RFTA with increasing additions of CBZ, recorded at 680 nm (B) and 380 nm (D). [CBZ] = 0-2 $\times 10^{-2}$ M. Stern-Volmer plot corresponding to data registered at 680 nm (C). The experiments were carried out in deaerated acetonitrile.

$$Quenching\ of\ {}^{3}(RFTA)^{*}\ by\ O_2\,(\%) = \frac{\frac{\Phi_{isc}}{\tau_s}}{\frac{\Phi_F}{\tau_s}+\frac{\Phi_{isc}}{\tau_s}+k_{qs}[Q]} x \frac{k_{O_2T}[O_2]}{\frac{1}{\tau_T}+k_{qT}[Q]+k_{O_2T}[O_2]} x100 \quad (6)$$

$$^{3}(RFTA)^{*}\ intrinsic\ decay\ (\%) = \frac{\frac{\Phi_{isc}}{\tau_s}}{\frac{\Phi_F}{\tau_s}+\frac{\Phi_{isc}}{\tau_s}+k_{qs}[Q]} x \frac{\frac{1}{\tau_T}}{\frac{1}{\tau_T}+k_{qT}[Q]+k_{O_2T}[O_2]} x100 \quad (7)$$

where k_{qS} and k_{qT} are the quenching constants of the singlet and triplet excited state of RFTA, [Q] the concentration of the drugs, Φ_F and Φ_{isc} are the quantum yields of fluorescence and intersystem crossing, τ_s and τ_T are the lifetime of the singlet and triplet excited state of RFTA, k_{O2T} is the quenching constant of oxygen (Fig. S12, $k_{qTO2} = 9.5 \times 10^9\ M^{-1}\ s^{-1}$) and $[O_2]$ is the concentration of oxygen in aerated acetonitrile ($[O_2] = 2.42 \times 10^{-3}$ M) [44].

Furthermore, considering the most optimistic situation in which 100% of the quenching of ^{3}RFTA* by O_2 gives rise to $^1O_2$, the contribution of the quenching of $^1O_2$ by CBZ and ATN *versus* $^1O_2$ intrinsic decay was calculated according to the following equations:

$$Quenching\ \ of\ \ {}^{1}O_2\ by\ the\ \ pollutants(\%) = \frac{\frac{\Phi_{isc}}{\tau_s}}{\frac{\Phi_F}{\tau_s}+\frac{\Phi_{isc}}{\tau_s}+k_{qs}[Q]} x \frac{k_{qTO_2}[O_2]}{\frac{1}{\tau_T}+k_{qT}[Q]+k_{qTO_2}[O_2]} x \frac{k_{q1O_2}[Q]}{\frac{1}{\tau_{1O_2}}+k_{q1O_2}[Q]} x100 \quad (8)$$

$$Intrinsic\ \ decay\ \ of\ \ {}^{1}O_2\ (\%) = \frac{\frac{\Phi_{isc}}{\tau_s}}{\frac{\Phi_F}{\tau_s}+\frac{\Phi_{isc}}{\tau_s}+k_{qs}[Q]} x \frac{k_{qTO_2}[O_2]}{\frac{1}{\tau_T}+k_{qT}[Q]+k_{qTO_2}[O_2]} x \frac{\frac{1}{\tau_{1O_2}}}{\frac{1}{\tau_{1O_2}}+k_{q1O_2}[Q]}\ x100 \quad (9)$$

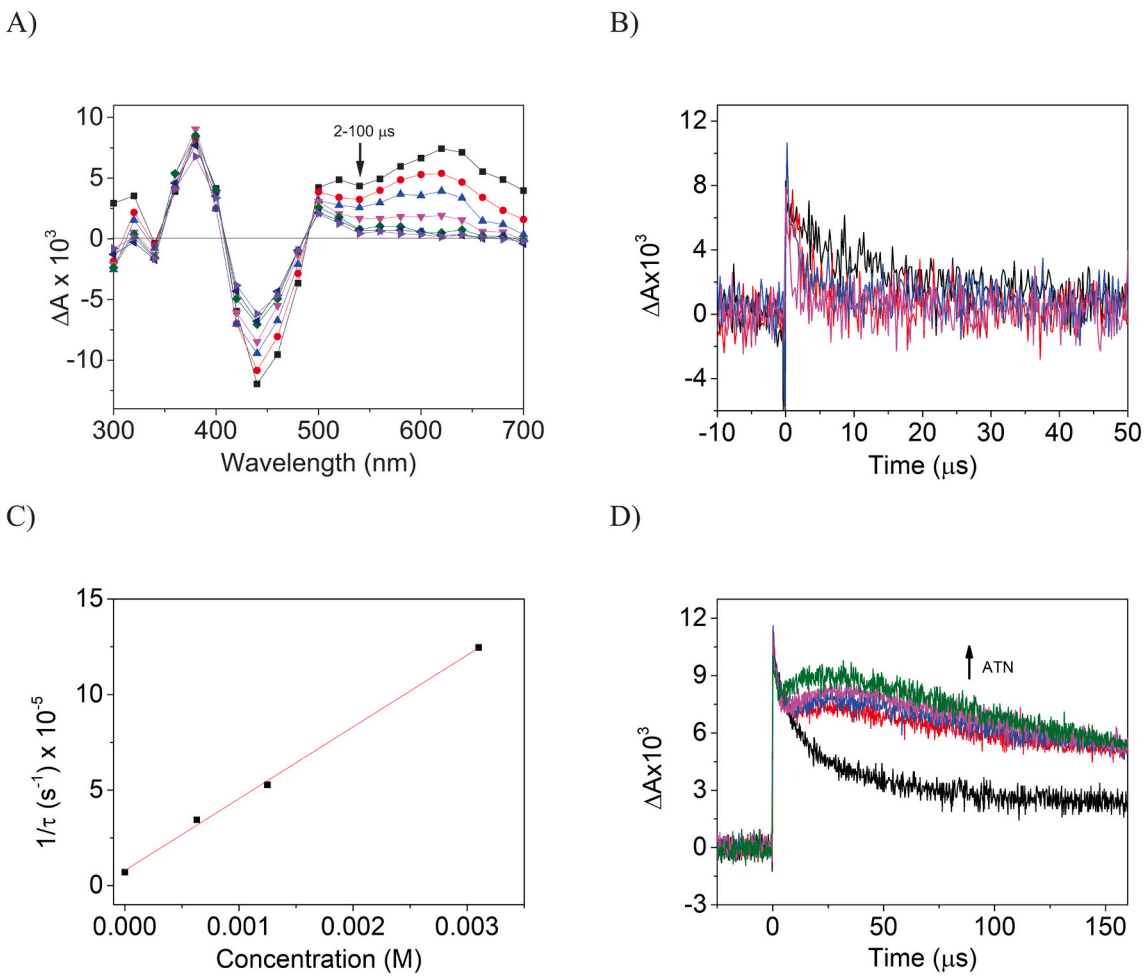

Fig. 7. Transient absorption spectra of RFTA and atenolol (1.9×10^{-3} M), recorded at different times after the laser pulse from 300 nm to 700 nm ($\lambda_{exc} = 355$ nm). (A) Transient absorption decays of RFTA in the presence of increasing additions of ATN, recorded at 680 nm (B) and 380 nm (D), ([ATN] = 0–3×10^{-3} M). Stern-Volmer plot resulting from the quenching experiment at 680 nm (C). The experiments were performed in deaerated acetonitrile.

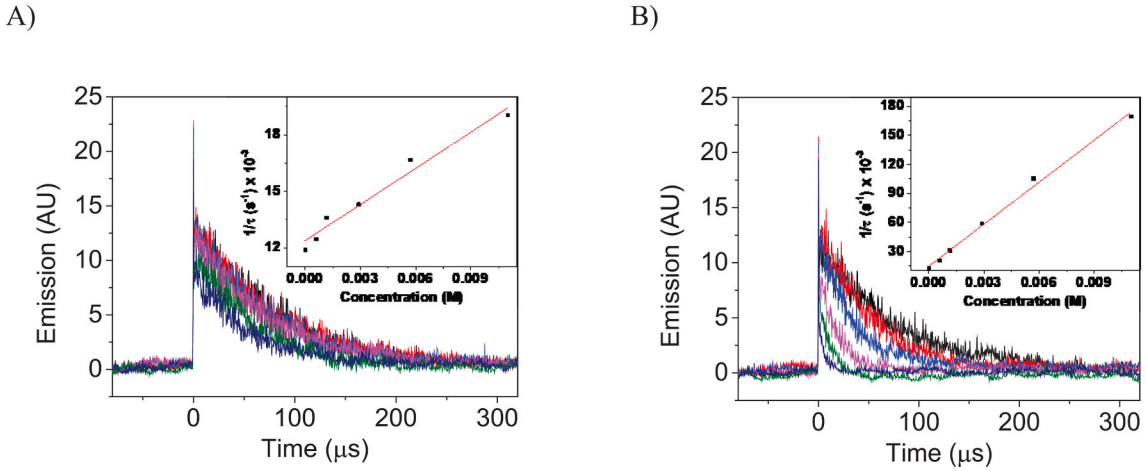

Fig. 8. Transient emission decays of $^1O_2$ generated upon laser flash excitation ($\lambda_{exc} = 355$ nm) of RFTA, and monitored at 1270 nm upon addition of different concentrations of CBZ (A) and ATN (B), ([CBA] and [ATN] = 0–1.1×10^{-2} M). Insets: corresponding Stern-Volmer plots. The experiments were performed in aerated acetonitrile.

Table 2
Relative weight of the quenching of the excited singlet and triplet states of RFTA and $^1O_2$ in the photolytic degradation of the drugs, at the indicated concentrations in acetonitrile.

[Q] (M)	Pollutant	Quenching of ^{1}(RFTA)* (%)	^{1}(RFTA)* intrinsic decay (%)	Quenching of ^{3}(RFTA)* (%)	^{3}(RFTA)* intrinsic decay (%)	Quenching of ^{3}(RFTA)* by O_2 (%)	Quenching of $^1O_2$ by the pollutants	$^1O_2$ intrinsic decay
10^{-3}	CBZ	0.49	52.74	0.02	0.13	46.62	2.32	44.30
	ATN	0.81	52.57	0.45	0.13	46.03	24.90	21.13
10^{-5}	CBZ	0.00	53.00	0.00	0.13	46.86	0.02	46.84
	ATN	0.01	53.00	0.00	0.13	46.86	0.55	46.31
10^{-8}	CBZ	0.00	53.00	0.00	0.13	46.87	0.00	46.87
	ATN	0.00	53.00	0.00	0.13	46.87	0.00	46.87

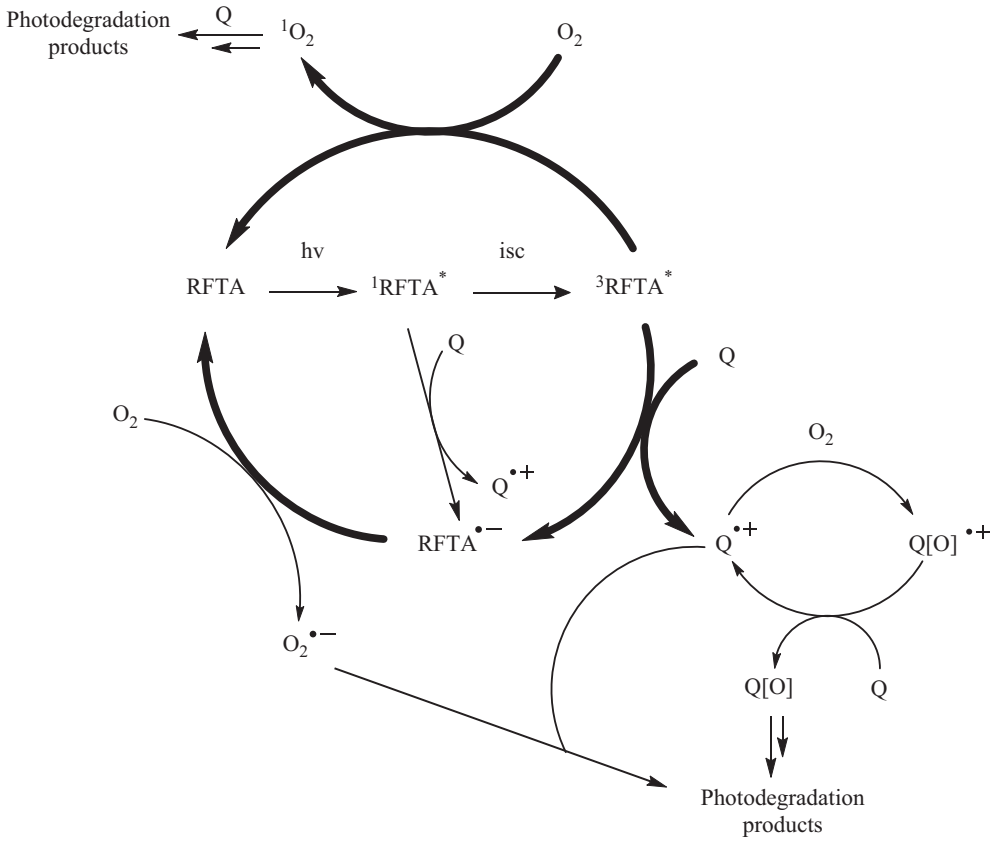

Scheme 3. Proposed photocatalytic degradation route of CBZ and ATN (Q) in the presence of RFTA and visible light.

where k_{q1O2} is the quenching constant of singlet oxygen by each pollutant (from experimental data k_{q1O2}= 6.4 × 10^5 M^{-1} s^{-1} for CBZ and k_{q1O2}= 1.4 × 10^7 M^{-1} s^{-1} for ATN), τ_{1O2} is the experimentally determined lifetime for $^1O_2$ in acetonitrile (81 μs), in good agreement with literature data [45], and [Q] is the concentration of each pollutant.

Taking into account the value of $\Phi_F = 0.53$ determined for RFTA in acetonitrile (see experimental section); $\Phi_{isc} = 0.47$ (calculated as 1- Φ_F); the experimentally determined k_{qS} and k_{qT} for CBZ (6.7 × 10^8 M^{-1} s^{-1} and 9.1 × 10^6 M^{-1} s^{-1}) and for ATN (1.1 × 10^9 M^{-1} s^{-1} and 3.7 × 10^8 M^{-1} s^{-1}); $\tau_S = 7.40 \times 10^{-9}$ s and $\tau_T = 1.5 \times 10^{-5}$ s of RFTA in acetonitrile, from emission and transient absorption time-resolved experiments; the relative contribution of ^{1}RFTA*, ^{3}RFTA* and $^1O_2$ in the quenching of the drugs is given in Table 2.

As expected, the efficiency of the excited states quenching decreases with decreasing drug concentration. From these results we can postulate a degradation mechanism as depicted in Scheme 3, in which RFTA upon absorption of light reaches the first singlet excited state that suffers partial quenching by the pollutants. Nevertheless, most of the singlets are converted into the triplet excited state upon intersystem crossing. On one hand, the triplet excited state accepts an electron of CBZ and ATN (Q) giving rise initially to a radical ion pair ^{3}(RFTA$^{\bullet-}$/Q$^{\bullet+}$) that lives long enough to separate into the radical anion of the photocatalyst (RFTA$^{\bullet-}$) and the radical cation of the drug (Q$^{\bullet+}$). The photocatalyst is recovered by subsequent reduction of molecular oxygen to reinitiate the cycle, while the radical cations resulting from the drugs react with O_2 starting a radical chain process responsible for the observed photodegradation products.

On the other hand, the ^{3}RFTA* reacts with oxygen in a triplet-triplet energy transfer process, giving rise to the ground state of RFTA and singlet oxygen, which is highly reactive, especially with ATN. Nevertheless, although Table 2 shows that photodegradation is mainly mediated by singlet oxygen, we are assuming that quenching of ^{3}RFTA* by O_2 results mainly in the formation of $^1O_2$. Besides, reaction between singlet oxygen and drugs is stoichiometric, while triplet excited state quenching by the drugs involves the formation of reactive radicals, able to initiate a chain reaction. Therefore, quenching of ^{3}RFTA* by the drugs is the chain initiation step and, depending on the chain length, could eventually lead to oxidation products much more efficiently than suggested at first sight by the numbers appearing in Table 2.

To better investigate the real contribution of electron transfer/singlet oxygen mechanisms we paid attention to the photodegradation rate and photoproducts obtained when photodegradation was performed in D_2O *vs* H_2O (to increase the prospects of $^1O_2$, since its lifetime in D_2O is *ca.* 51 μs *vs* 3.5 μs in H_2O) [45,46]. Results obtained showed that the photodegradation was slightly slower when performed in D_2O. Moreover, the main photoproducts were the same in the two solvents (see Section 2 in the Supplementary material, Figs. S2–S11). Furthermore, photodegradation of the drugs was performed in the presence of triphenylpyrylium a photosensitizer known to produce photooxygenation of 1,2-diarylethylenes although it does not generate singlet oxygen nor superoxide anion [47,48]. In this case, the same photoproducts profile was observed, which acted as a proof of evidence of the main contribution of the electron transfer mechanism in the photodegradation of CBZ and ATN (see Figs. S2–S10).

4. Conclusions

Acetylated riboflavin (RFTA), in the presence of solar light, works as an excellent photocatalyst able to produce photodegradation of recalcitrant drugs, such as carbamazepine and atenolol, in <2 h. Specifically, two oxidative pathways operating at a time are responsible for the degradation: i) direct oxidation of CBZ and ATN by singlet oxygen, and ii) e^- transfer to the triplet excited state of RFTA, giving rise to the formation of photooxidized radical cations, that in the presence of oxygen are able to participate in chain reactions and eventually evolve to the photoproducts. Experiments performed in D_2O or in the presence of triphenylpyrylium as a photocatalyst gave rise to the same photoproducts profile, supporting the main contribution of the electron transfer mechanism in the photodegradation of CBZ and ATN. A detailed analysis of the resulting products performed by UFLC combined with MS^2 is in agreement with the postulated photocatalytic degradation mechanism.

Declaration of Competing Interest

The authors declare no conflict of interest.

Acknowledgements

Financial support from H2020/Marie Skłodowska-Curie Actions under the AQUAlity project (Reference: 765860), Consellería d'Educació, Investigació, Cultura i Esport (PROMETEO/2017/075) and the Spanish Ministry of Science, Innovation and Universities (PID2019-110441RB-C33) is gratefully acknowledged.

Appendix A. Supplementary data

Supplementary data to this article can be found online at https://doi.org/10.1016/j.jphotobiol.2021.112250.

References

[1] E. Ben Mordechay, J. Tarchitzky, Y. Chen, M. Shenker, B. Chefetz, Composted biosolids and treated wastewater as sources of pharmaceuticals and personal care products for plant uptake: a case study with carbamazepine, Environ. Pollut. 232 (2018) 164–172, https://doi.org/10.1016/j.envpol.2017.09.029.

[2] T. Rasheed, M. Bilal, A.A. Hassan, F. Nabeel, R.N. Bharagava, L.F. Romanholo Ferreira, H.N. Tran, H.M.N. Iqbal, Environmental threatening concern and efficient removal of pharmaceutically active compounds using metal-organic frameworks as adsorbents, Environ. Res. 185 (2020) 109436, https://doi.org/10.1016/j.envres.2020.109436.

[3] C.R. Ohoro, A.O. Adeniji, A.I. Okoh, O.O. Okoh, Distribution and chemical analysis of pharmaceuticals and personal care products (PPCPs) in the environmental systems: a review, Int. J. Environ. Res. Public Health 16 (2019), https://doi.org/10.3390/ijerph16173026.

[4] D.R. Baker, B. Kasprzyk-Hordern, Critical evaluation of methodology commonly used in sample collection, storage and preparation for the analysis of pharmaceuticals and illicit drugs in surface water and wastewater by solid phase extraction and liquid chromatography-mass spectrometry, J. Chromatogr. A 1218 (2011) 8036–8059, https://doi.org/10.1016/j.chroma.2011.09.012.

[5] F. Pomati, S. Castiglioni, E. Zuccato, R. Fanelli, D. Vigetti, C. Rossetti, D. Calamari, Effects of a complex mixture of therapeutic drugs at environmental levels on human embryonic cells, Environ. Sci. Technol. 40 (2006) 2442–2447, https://doi.org/10.1021/es051715a.

[6] P. Fernández-Castro, M. Vallejo, M.F. San Román, I. Ortiz, Insight on the fundamentals of advanced oxidation processes: role and review of the determination methods of reactive oxygen species, J. Chem. Technol. Biotechnol. 90 (2015) 796–820, https://doi.org/10.1002/jctb.4634.

[7] A.R. Ribeiro, O.C. Nunes, M.F.R. Pereira, A.M.T. Silva, An overview on the advanced oxidation processes applied for the treatment of water pollutants defined in the recently launched directive 2013/39/EU, Environ. Int. 75 (2015) 33–51, https://doi.org/10.1016/j.envint.2014.10.027.

[8] S. Giannakis, S. Rtimi, C. Pulgarin, Light-assisted advanced oxidation processes for the elimination of chemical and microbiological pollution of wastewaters in developed and developing countries, Molecules 22 (2017) 1070, https://doi.org/10.3390/molecules22071070.

[9] M.L. Marin, L. Santos-Juanes, A. Arques, A.M. Amat, M.A. Miranda, Organic photocatalysts for the oxidation of pollutants and model compounds, Chem. Rev. 112 (2012) 1710–1750, https://doi.org/10.1021/cr2000543.

[10] M.A. Fox, M.T. Dulay, Heterogeneous photocatalysis, Chem. Rev. 93 (1993) 341–357, https://doi.org/10.1021/cr00017a016.

[11] W.K. Jo, R.J. Tayade, New generation energy-efficient light source for photocatalysis: LEDs for environmental applications, Ind. Eng. Chem. Res. 53 (2014) 2073–2084, https://doi.org/10.1021/ie404176g.

[12] Y. Jin, L. Ou, H. Yang, H. Fu, Visible-light-mediated aerobic oxidation of N-alkylpyridinium salts under organic photocatalysis, J. Am. Chem. Soc. 139 (2017) 14237–14243, https://doi.org/10.1021/jacs.7b07883.

[13] T.P. Yoon, M.A. Ischay, J. Du, Visible light photocatalysis as a greener approach to photochemical synthesis, Nat. Chem. 2 (2010) 527–532, https://doi.org/10.1038/nchem.687.

[14] M. Marin, M.A. Miranda, M.L. Marin, A comprehensive mechanistic study on the visible-light photocatalytic reductive dehalogenation of haloaromatics mediated by Ru(bpy)3Cl2, Catal. Sci. Technol. 7 (2017) 4852–4858, https://doi.org/10.1039/c7cy01231d.

[15] R. Martinez-Haya, J. Gomis, A. Arques, A.M. Amat, M.A. Miranda, M.L. Marin, Direct detection of the triphenylpyrylium-derived short-lived intermediates in the photocatalyzed degradation of acetaminophen, acetamiprid, caffeine and carbamazepine, J. Hazard. Mater. 356 (2018) 91–97, https://doi.org/10.1016/j.jhazmat.2018.05.023.

[16] J. Meng, F. Xu, S. Yuan, Y. Mu, W. Wang, Z.H. Hu, Photocatalytic oxidation of roxarsone using riboflavin-derivative as a photosensitizer, Chem. Eng. J. 355 (2019) 130–136, https://doi.org/10.1016/j.cej.2018.08.127.

[17] A. Wolnicka-Glubisz, A. Pawlak, M. Insinska-Rak, A. Zadlo, Analysis of photoreactivity and phototoxicity of riboflavin's analogue 3MeTARF, J. Photochem. Photobiol. B Biol. 205 (2020) 111820, https://doi.org/10.1016/j.jphotobiol.2020.111820.

[18] R. Martinez-Haya, M.A. Miranda, M.L. Marin, Metal-free photocatalytic reductive dehalogenation using visible-light: a time-resolved mechanistic study, Eur. J. Org. Chem. 2017 (2017) 2164–2169, https://doi.org/10.1002/ejoc.201601494.

[19] R. Martinez-Haya, M.A. Miranda, M.L. Marin, Type I vs type II photodegradation of pollutants, Catal. Today 313 (2018) 161–166, https://doi.org/10.1016/j.cattod.2017.10.034.

[20] C.K. Remucal, K. McNeill, Photosensitized amino acid degradation in the presence of riboflavin and its derivatives, Environ. Sci. Technol. 45 (2011) 5230–5237, https://doi.org/10.1021/es200411a.

[21] D.U. Mccormick, Flavin derivatives via bromination of the 8-methyl Substituent (1), J. Heterocyclic Chem. 7 (1970) 447–450, https://doi.org/10.1002/jhet.5570070240C.

[22] B.J. Fritz, S. Kasai, K. Matsui, Photochemical properties of flavin derivatives, Photochem. Photobiol. 45 (1987) 113–117, https://doi.org/10.1111/j.1751-1097.1987.tb08411.x.

[23] R.A. Larson, P.L. Stackhouse, T.O. Crowley, Riboflavin tetraacetate: a potentially useful photosensitizing agent for the treatment of contaminated waters, Environ. Sci. Technol. 26 (1992) 1792–1798, https://doi.org/10.1021/es00033a013.

[24] P. Calza, C. Medana, E. Padovano, V. Giancotti, C. Baiocchi, Identification of the unknown transformation products derived from clarithromycin and carbamazepine using liquid chromatography/high-resolution mass spectrometry, Rapid Commun. Mass Spectrom. 26 (2012) 1687–1704, https://doi.org/10.1002/rcm.6279.

[25] Y. Tian, X. Xia, J. Wang, L. Zhu, J. Wang, F. Zhang, Z. Ahmad, Chronic toxicological effects of carbamazepine on Daphnia magna Straus: effects on reproduction traits, body length, and intrinsic growth, Bull. Environ. Contam. Toxicol. 103 (2019) 723–728, https://doi.org/10.1007/s00128-019-02715-w.

[26] R. Andreozzi, R. Marotta, G. Pinto, A. Pollio, Carbamazepine in water: persistence in the environment, ozonation treatment and preliminary assessment on algal toxicity, Water Res. 36 (2002) 2869–2877, https://doi.org/10.1016/S0043-1354(01)00500-0.

[27] S. Batra, R. Bhushan, Bioassay, determination and separation of enantiomers of atenolol by direct and indirect approaches using liquid chromatography: a review, Biomed. Chromatogr. 32 (2018) 1–21, https://doi.org/10.1002/bmc.4090.

[28] A.A. Godoy, F. Kummrow, P.A.Z. Pamplin, Occurrence, ecotoxicological effects and risk assessment of antihypertensive pharmaceutical residues in the aquatic environment - a review, Chemosphere 138 (2015) 281–291, https://doi.org/10.1016/j.chemosphere.2015.06.024.

[29] P.F. Heelis, The photophysical and photochemical properties of flavins (isoalloxazines), Chem. Soc. Rev. 11 (1982) 15–39, https://doi.org/10.1039/CS9821100015.

[30] G. Weber, F.W.J. Teale, Determination of the absolute quantum yield of fluorescent solutions, Trans. Faraday Soc. 53 (1957) 646–655, https://doi.org/10.1039/tf9575300646.
[31] M.A. Sheraz, S.H. Kazi, S. Ahmed, Z. Anwar, I. Ahmad, Photo, thermal and chemical degradation of riboflavin, Beilstein J. Org. Chem. 10 (2014) 1999–2012, https://doi.org/10.3762/bjoc.10.208.
[32] I. Ahmad, T. Mirza, S.G. Musharraf, Z. Anwar, M.A. Sheraz, S. Ahmed, M.A. Ejaz, A. Khurshid, Photolysis of carboxymethylflavin in aqueous and organic solvent: a kinetic study, RSC Adv. 9 (2019) 26559–26571, https://doi.org/10.1039/c9ra02818h.
[33] H. Cui, H.M. Hwang, S. Cook, K. Zeng, Effect of photosensitizer riboflavin on the fate of 2,4,6-trinitrotoluene in a freshwater environment, Chemosphere. 44 (2001) 621–625, https://doi.org/10.1016/S0045-6535(00)00333-7.
[34] J.S. Stanojević, J.B. Zvezdanović, D.Z. Marković, Riboflavin degradation in the presence of quercetin in methanol under continuous UV-B irradiation: the ESI-MS-UHPLC analysis, Monatshefte Fur Chemie 146 (2015) 1787–1794, https://doi.org/10.1007/s00706-015-1561-1.
[35] I. Ahmad, T. Mirza, Z. Anwar, S. Ahmed, M.A. Sheraz, M.A. Ejaz, S.H. Kazi, Photodegradation of formylmethylflavin by side–chain and isoalloxazine ring cleavage in alkaline solution: a kinetic study, J. Photochem. Photobiol. A Chem. 374 (2019) 106–114, https://doi.org/10.1016/j.jphotochem.2019.01.028.
[36] S. Castiglioni, R. Bagnati, D. Calamari, R. Fanelli, E. Zuccato, A multiresidue analytical method using solid-phase extraction and high-pressure liquid chromatography tandem mass spectrometry to measure pharmaceuticals of different therapeutic classes in urban wastewaters, J. Chromatogr. A 1092 (2005) 206–215, https://doi.org/10.1016/j.chroma.2005.07.012.
[37] R. Andreozzi, R. Marotta, N. Paxéus, Pharmaceuticals in STP effluents and their solar photodegradation in aquatic environment, Chemosphere 50 (2003) 1319–1330, https://doi.org/10.1016/S0045-6535(02)00769-5.
[38] C.M.C.L. Martínez, M.I. Fernández, J.A. Santaballa, J. Faria, Kinetics and mechanism of aqueous degradation of carbamazepine by heterogeneous photocatalysis using nanocrystalline TiO2, ZnO and multi-walled carbon nanotubes-anatase composites, Appl. Catal. B Environ. 102 (2011) 563–571, https://doi.org/10.1016/j.apcatb.2010.12.039.
[39] S. Chiron, C. Minero, D. Vione, Photodegradation processes of the antiepileptic drug carbamazepine, relevant to estuarine waters, Environ. Sci. Technol. 40 (2006) 5977–5983, https://doi.org/10.1021/es060502y.
[40] C.B.C. Medana, P. Calza, F. Carbone, E. Pelizzetti, H. Hidaka, Characterization of atenolol transformation products onlight-activated TiO2surface by high-performance liquidchromatography/high-resolution mass spectrometry, Rapid Commun. Mass Spectrom. 22 (2008) 301–313, https://doi.org/10.1002/rcm.3370.
[41] J. Radjenović, C. Sirtori, M. Petrović, D. Barceló, S. Malato, Solar photocatalytic degradation of persistent pharmaceuticals at pilot-scale: kinetics and characterization of major intermediate products, Appl. Catal. B Environ. 89 (2009) 255–264, https://doi.org/10.1016/j.apcatb.2009.02.013.
[42] Y. Ji, L. Zhou, C. Ferronato, X. Yang, A. Salvador, C. Zeng, J.M. Chovelon, Photocatalytic degradation of atenolol in aqueous titanium dioxide suspensions: kinetics, intermediates and degradation pathways, J. Photochem. Photobiol. A Chem. 254 (2013) 35–44, https://doi.org/10.1016/j.jphotochem.2013.01.003.
[43] L.K. Fraiji, D.M. Hayes, T.C. Werner, Static and dynamic fluorescence quenching experiments for the physical chemistry laboratory, J. Chem. Educ. 69 (1992) 424–428, https://doi.org/10.1021/ed069p424.
[44] M. Quaranta, M. Murkovic, I. Klimant, A new method to measure oxygen solubility in organic solvents through optical oxygen sensing, Analyst. 138 (2013) 6243–6245, https://doi.org/10.1039/c3an36782g.
[45] J.R. Hurst, J.D. McDonald, G.B. Schuster, Lifetime of singlet oxygen in solution directly determined by laser spectroscopy, J. Am. Chem. Soc. 104 (1982) 2065–2067, https://doi.org/10.1021/ja00371a065.
[46] J. Baier, Time dependence of singlet oxygen luminescence provides an indication of oxygen concentration during oxygen consumption, J. Biomed. Opt. 12 (2007), 064008, https://doi.org/10.1117/1.2821153.
[47] H. Garcia, M.A. Miranda, F. Mojarrad, M.-J. Sabater, Involvement of oxirane intermediates in the electron transfer photooxygenation of 1,1- and 1,2-diaryl-ethylenes sensitized by 2,4,6-triphenylpyrylium tetrafluoroborate, Tetrahedron 50 (1994) 8773–8780, https://doi.org/10.1016/S0040-4020(01)85351-5.
[48] M.A. Miranda, H. Garcia, 2,4,6-Triphenylpyrylium tetrafluoroborate as an electron-transfer photosensitizer, Chem. Rev. 94 (1994) 1063–1089, https://doi.org/10.1021/cr00028a009.